Electrospun nanofiber films suppress inflammation in vitro and eradicate endodontic bacterial infection in an E. faecalis infected ex vivo human tooth culture model

Journal:	*ACS Biomaterials Science & Engineering*
Manuscript ID	ab-2022-00150h
Manuscript Type:	Article
Date Submitted by the Author:	08-Feb-2022
Complete List of Authors:	Chachlioutaki, Konstantina; Aristotle University of Thessaloniki, School of pharmacy Karavasili, Christina; Aristotle University of Thessaloniki, Laboratory of Pharmaceutical Technology, Department of Pharmaceutical Sciences Adamoudi, Elisavet ; School of Dentistry, Faculty of Health Sciences, Aristotle University of Thessaloniki Tsitsos, Anestis ; Aristotle University of Thessaloniki Economou, Vangelis ; Aristotle University of Thessaloniki Beltes, Charis ; Aristotle University of Thessaloniki Bouropoulos, Nikolaos; University of Patras, Materials Science Katsamenis, Orestis; University of Southampton, μ-VIS X-ray Imaging Centre Doherty, Regan; University Hospital Southampton NHS Foundation Trust Bakopoulou, Athina ; Aristotle University of Thessaloniki Fatouros, Dimitrios; Aristotle University of Thessaloniki, School of Pharmacy

Electrospun nanofiber films suppress inflammation *in vitro* and eradicate endodontic bacterial infection in an *E. faecalis* infected *ex vivo* human tooth culture model

Konstantina Chachlioutaki[#], Christina Karavasili[#], Elisavet Adamoudi[¶], Anestis Tsitsos[‡], Vangelis Economou[‡], Charis Beltes[§], Nikolaos Bouropoulos[∞],[■], Orestis L. Katsamenis[ǀ], Regan Doherty[&], Athina Bakopoulou[¶], Dimitrios G. Fatouros[#],[*]

[#]*Department of Pharmacy, Division of Pharmaceutical Technology, Aristotle University of Thessaloniki, Thessaloniki, GR-54124, Greece*

[¶]*Department of Prosthodontics, School of Dentistry, Faculty of Health Sciences, Aristotle University of Thessaloniki, Thessaloniki, GR-54124, Greece*

[‡]*Laboratory of Hygiene of Foods of Animal Origin - Veterinary Public Health, School of Veterinary Medicine, Faculty of Health Sciences, Aristotle University of Thessaloniki, Thessaloniki GR-54124, Greece*

[§]*Department of Endodontics, School of Dentistry, Faculty of Health Sciences, Aristotle University of Thessaloniki, Thessaloniki, GR-54124, Greece*

[∞]*Department of Materials Science, University of Patras, 26504 Rio, Patras, Greece*

▪*Foundation for Research and Technology Hellas, Institute of Chemical Engineering and High Temperature Chemical Processes, 26504 Patras, Greece*

[‡]*μ-VIS X-ray Imaging Centre, Faculty of Engineering and Physical Sciences, University of Southampton, Southampton, SO17 1BJ, United Kingdom*

[&]*Biomedical Imaging Unit, University Hospital Southampton NHS Trust, Southampton, SO16 6YD, United Kingdom*

KEYWORDS: electrospun films, anti-inflammatory, antimicrobial, root canal treatment, ketoprofen, ZnO nanoparticles, *E. faecalis*

ABSTRACT

Treatment failure of endodontic infections and their concurrent inflammations is commonly associated with microbial persistence and reinfection, also stemming from the anatomical restrictions of the root canal system. Aiming to address the shortcomings of current treatment options, a fast-disintegrating nanofibrous film was developed for the intracanal co-administration of an antimicrobial (ZnO nanoparticles) and an anti-inflammatory (ketoprofen) agent. The electrospun films were fabricated based on polymers that dissolve rapidly to constitute the actives readily available at the site of action, aiming to eliminate both microbial infection and inflammation. The anti-inflammatory potency of the nanofiber films was assessed in an *in vitro* model of LPS-simulated RAW 264.7 cells, after confirming their biocompatibility in the same cell line. The nanofiber films were found effective against *Enterococcus faecalis*, one of the most prominent pathogens inside the root canal space, both *in vitro* and *ex vivo* using a human tooth model experimentally infected with *E. faecalis*. The physical properties and antibacterial and anti-

inflammatory potency of the proposed electrospun nanofiber films constitute a promising therapeutic module in endodontic therapy of non-vital infected teeth. All manuscripts must be accompanied by an abstract. The abstract should briefly state the problem or purpose of the research, indicate the theoretical or experimental plan used, summarize the principal findings, and point out major conclusions.

INTRODUCTION

Endodontic infection is a biofilm-based disease of the root canal space modulated by the virulence of the endogenous complex microbiota[1]. Accompanied by concurrent inflammation, root canal infection can occur due to untreated dental caries, trauma or periodontal disease and may lead to the establishment of apical periodontitis[2]. Therapeutic interventions are based on chemo-mechanical debridement to facilitate biofilm disruption and eradication. Nevertheless, endodontic

treatment failure may occur due to microbial persistence and reinfection, also stemming from the anatomical restrictions of the root canal system hindering adequate debridement and disinfectant infiltration[3].

Guidelines on dental infection management recommend triple antibiotic paste (TAP), consisting of a mixture of ciprofloxacin, metronidazole and minocycline[4]. Despite its antimicrobial efficacy, TAP may produce complications related to bacterial resistance, tissue irritation, stem cell toxicity and teeth discoloration, due to its acidic nature[5]. Additional irrigation practices include the use of sodium hypochlorite (NaOCl) or the less caustic chlorhexidine, the efficacy of which is, however, compromised by the damaging effect of NaOCl on the dentin matrix and periapical tissues and the formation of bacterial persisters or chlorhexidine's inability to dissolve necrotic tissues and reduced efficacy against Gram (-) bacteria[2]. These limitations gave prominence to the use of nanoparticle-based irrigants, such as silver (Ag) or zinc oxide (ZnO) nanoparticles (NPs), both having a similar mode of bactericidal action[6]. Equally important to eliminating endodontic microbial infection is the management of inflammation caused by bacterial infections. Ketoprofen is one of the most widely used non-steroidal anti-inflammatory agents (NSAIDs) administered orally for the management of inflammation and post-operative endodontic pain[7]. Systemic

administration of NSAIDs, however, may not achieve sufficient and immediate pain relief, while at the same time non-specific drug distribution is unavoidable.

In light of these shortcomings, there has been an increasing interest in novel drug delivery systems for the endodontic administration of anti-inflammatory and antimicrobial agents, as well as in novel approaches, such as the application of pulsed magnetic field as a bacteriostatic stimulus against *Enterococcus faecalis* during root canal treatment[8]. Several clinical reports have demonstrated the potential of electrospun films as a suitable drug delivery platform for dental applications[9]. Within this context, intracanal administration of antibacterial TAP-mimic electrospun scaffolds based on polydioxanone aimed to achieve disinfection of the root canal system, yet without the tooth discoloration occurring upon TAP application[10,11,12]. Curcumin incorporation within the same electrospun polymer matrix aimed to serve as an alternative to TAP for root canal disinfection[13], while chlorhexidine loading in polyvinyl alcohol (PVA)-based scaffolds was intended for use in vital pulp therapy[14]. The introduction of nanoparticle-based antimicrobials (Ag, ZnO) in electrospun scaffolds has also been applied mainly for periodontal administration[15,16]. Nevertheless, there have been very few reports on a single drug delivery system

that fulfill the antimicrobial, anti-inflammatory, and post-operative pain relief requirements for root canal treatment, including the TAP containing the anti-inflammatory drug catafast[17].

Aiming to address these requirements, the current study describes the development and characterization of an electrospun nanofibrous film for the intracanal co-administration of an antimicrobial (ZnO NPs) and an anti-inflammatory (ketoprofen) agent. The nanofibrous matrix was fabricated based on polymers that dissolve rapidly to constitute the actives readily available at the site of action, aiming to eliminate both microbial infection and inflammation. For that reason, PVA was selected as a hydrophilic, bioadhesive, biocompatible, and biodegradable polymer[18], along with two cellulose derivatives, namely hydroxypropyl methylcellulose (HPMC) and carboxymethylcellulose (CMC), widely used for their excellent film-forming, mechanical and adhesive properties[19,20].

MATERIALS AND METHODS

Materials. Polyvinyl alcohol (PVA, Mowiol® 8-88 Mw ~67,000), hydroxypropylmethyl cellulose (HPMC, Hyrpomellose 2910) and carboxymethyl cellulose [CMC, 400-800 cP, 2% in H_2O (25 ˚C)(lit.)], zinc acetate dihydrate ($Zn(CH_3COO)_2{\cdot}2H_2O$), potassium hydroxide (KOH), and

methanol were purchased from Sigma-Aldrich Corp. (Steinheim, Germany). Ketoprofen (Keto) was obtained from Fagron Hellas (Athens, Greece). All reagents were of analytical grade and were used as received.

Synthesis of ZnO nanoparticles. Seven g zinc acetate dihydrate were transferred into a three-neck spherical flask equipped with a condenser containing 500 mL methanol. The suspension was heated at 65 ^{o}C under magnetic stirring. Next, 2.43 g potassium hydroxide were added, and the solution was heated to boiling. Since the boiling point of methanol is at 65 ^{o}C the temperature remained constant during the reaction. After 4 h, the suspension was cooled down at room temperature (RT) and remained with the mother liquid for 4 days before centrifugation at 3000 rpm for 30 min. The pellet was resuspended three times with methanol and finally dried at RT.

Preparation of the spinning solutions and electrospinning process. PVA, HPMC and CMC were the polymers used to obtain the nanofibrous films. The composition of the prepared solutions is reported in Table S1. Briefly, PVA was dissolved in deionized water under magnetic stirring at 80^{o}C for 2 h prior to the addition of HPMC and CMC. Ketoprofen was dissolved in DMF and ZnO

NPs were added in the same solution and briefly sonicated until homogenously dispersed. The two solutions were mixed at a 1:1 volume ratio and were magnetically stirred for 2 h. Control samples were prepared following the same procedure as described above in the absence of ketoprofen and ZnO. The electrospinning apparatus used was the same as in previous studies[21]. The polymeric solutions were loaded in plastic syringes (10 mL) that were attached to a capillary tip (21G) and an electrode was clipped to the nozzle system. The solutions were pumped at a feed rate of 0.3 mL/h, the voltage was set at 20 kV, and the distance between the needle tip and the grounded collector was set at 15 cm. The electrospun films were collected and stored in a desiccator.

Characterization of ZnO nanoparticles and the nanofibrous films

Morphological assessment. Morphological characterization of ZnO NPs was performed using Transmission Electron Microscopy (TEM) (JEM 2100, JEOL, Japan). For the preparation of TEM specimens, about 1 mg of ZnO powder was dispersed in 2 mL ethanol and the suspension was sonicated in a bath sonicator for 15 min. Next, a drop of the suspension was transferred on a carbon-coated grid and evaporated. The size of the crystals was measured from the corresponding TEM images after measuring 65 particles using the image analysis software ImageJ. Fiber

morphology was assessed by means of SEM (field emission scanning electron microscope, LEO 1530VP). The specimens were mounted on metallic sample stands using conductive double-sided carbon adhesive tape (PELCO Image Tabs) and coated by gold using a BAL-TECSCD-004 sputtering unit. The accelerating voltage was set at 15 kV. Fiber diameter distribution was determined by analyzing at least 100 randomly selected fibers from three different SEM images using ImageTool software (UTHSCSA,Version 3.00) to calculate the average fiber diameter. Morphological characterization of the ZnO-containing nanofibers was conducted by means of TEM imaging using a 120 kV Hitachi HT7700 Transmission Electron Microscope with a LaB6 filament, equipped with an AMT XR81 direct mount camera. The nanofibers were directly deposited onto the TEM grid using the electrospinning process described above. The loaded grids were then loaded into the microscope where an area of interest and appropriate magnification was selected. For the tilt series, used here to confirm NPs location with respect to fibers' surface, were generated by tilting the sample from 0˚ to 60˚ then -60˚, imaging at 1.5˚ intervals, using SerialEM automated tilt series acquisition software. The resulting image stack was processed using the Etomo programme within IMOD to create an aligned tilt series.

Physicochemical characterization studies. The thermal properties of the raw materials and the electrospun films were evaluated on a DSC 204 F1 Phoenix apparatus (NETZSCH, Germany). Samples were weighed in aluminum pans with perforated lids and heated from 25 °C to 200 °C at a rate of 10 °C/min under nitrogen gas flow of 70 mL/min. The purity and the mean size of the synthesized ZnO NPs, as well as the crystallinity of the raw materials and the electrospun films were assessed with XRD analysis. The diffraction spectra of the samples were acquired on a D8-Advance diffractometer (Bruker, Germany) with Ni-filtered CuKa1 radiation (40 kV, 40 mA) and were recorded from 5° to 60°, at a step size of 0.02° and at a scanning speed of 0.5 s/step.

***In vitro* disintegration time**. Disintegration time was estimated based on a previously established procedure [21]. Briefly, a piece of filter paper was placed in a petri dish (diameter: 10 cm) containing 2 mL of simulated salivary fluid (SSF)[22]. The electrospun films were cut in circles (diameter: 25 mm) and placed on the wet paper. The procedure was recorded with a video camera and the time required for complete disintegration to occur was estimated after video conversion to JPEG images corresponding to specified time-points post film wetting.

Drug content quantification and *in vitro* dissolution study. The drug content of each formulation was calculated after quantification with HPLC analysis. The dissolution profile of ketoprofen from the electrospun films was recorded in SSF pH 6.8 at 37 °C in the presence of 0.5% v/v Tween 80 to assure sink conditions. The films (20 mg) were immersed in glass vials containing preheated SSF in a water bath at 37 °C. Samples (500 μL) were withdrawn and replaced by an equal volume of medium. The samples were centrifugated at 4000 rpm for 15 min and ketoprofen was quantified in the supernatants by HPLC analysis.

High-performance liquid chromatography Assay (HPLC). Ketoprofen quantification was performed using a HPLC system consisting of a pump (LC-10 AD VP), an auto-sampler (SIL-20A HT) equipped with a 100 µL loop and a UV–vis detector model SPD-10A VP (Shimadzu, Kyoto, Japan). A Discovery® HS C18 column (15 cm x 4.6 mm, 5 mm) was used and the mobile phase consisted of acetonitrile: 0.02 M KH2PO4 pH 3.0 70:30 v/v. The flow rate was set at 1.0 mL/min, the wavelength at 254 nm the injection volume was 20 µL. Under the described chromatographic conditions, the retention time of ketoprofen was approximately 3.2 min. Calibration curve of ketoprofen in SSF was linear (R^2=0.999) in the range of 20-100 µg/mL.

In Vitro Assays in Eucaryotic Cells

Cell culture conditions. RAW 264.7 cells, a murine macrophage cell line (ATCC, VA, USA), were cultured in complete culture medium (CCM) consisting of high glucose (4.5 g/L) Dulbecco's Modified Eagle's Medium (DMEM, Invitrogen, Karlsruhe, Germany), supplemented with 10% fetal Bovine Serum (FBS) (Invitrogen) and 1% of an antibiotic mixture (10,000 U/mL Penicillin, 10 mg/mL Streptomycin, 25 µg/mL Amphotericin B, Invitrogen), and incubated at 37 ˚C under a humidified atmosphere of 5% CO_2.

***In vitro* cell viability assay**. Cell viability/proliferation of RAW 264.7 cells exposed to the different electrospun films was determined using the MTT [3-(4, 5-dimethylthiazol-2-yl)-2,5-

diphenyltetrazolium bromide] assay. RAW 264.7 cells were plated at a density of 2×10^3 cells/well into 96-well plates containing 200 μL/well of CCM and incubated at 37˚C and 5% CO_2 overnight to allow cell attachment. Then, the culture medium was discarded and the films containing 5 different ketoprofen concentrations (0.01-, 0.05-, 0.1-, 0.5- and 1 mg/mL) were dissolved in fresh medium and added in each well containing cells (200 μL/well, n=6). After 24-, 48-, and 72 h fresh medium with 10% MTT (5 mg/mL in PBS) was added in each well and incubated for 4 h at 37°C and 5% CO_2. After this period, the medium containing the MTT solution was discarded, and DMSO was added to the wells for 1 h at 37 °C to dissolve the formazan crystals. The absorbance was measured against blank (DMSO) at a wavelength of 545 nm and a reference filter of 630 nm with a spectrophotometer (Epock, Biotek, Biotek Instruments, Inc, Vermont, USA). As controls, untreated RAW 264.7 cells, incubated under the same conditions, were used. Values were calculated as % percentage of the control RAW 264.7 cell values.

Gene expression analysis of pro-and anti-inflammatory markers of RAW 264.7 cells. To assess the biological effects of the different types of the electrospun films loaded with ketoprofen, focusing on their potential anti-inflammatory action, an in vitro model of Lipopolysaccharide

(LPS)-stimulated RAW 246.7 murine macrophages was used. In detail, RAW 264.7 cells were cultured in CMM as described in the section In vitro cell viability assay. Then, the cells were seeded in 12 well-plates (2 x10^5 cells/well) and incubated with fresh CCM overnight to allow initial cell attachment. Then, cells were stimulated with 1 μg/mL of the common bacterial endotoxin LPS for 3 h in high glucose DMEM containing the antibiotic mixture, but devoid of FBS (i.e., under serum deprivation conditions). Subsequently, the culture medium was replaced by each of the electrospun film groups containing ZnO nanoparticles and 0.1 mg/mL ketoprofen dissolved in fresh CCM, followed by incubation at 37˚C and 5% CO_2. The effects of the different electrospun films were assessed by real-time PCR analysis of the expression of several pro-inflammatory markers, including metalloproteinase (MMP)-3, MMP-9, MMP-13, monocyte chemoattractant protein-1 (MCP-1), interleukin (IL)-6, and the anti-inflammatory marker IL-10 after 24 h and 48 h. LPS-stimulated RAW 264.7 cells incubated under the same conditions but without exposure to the electrospun films and were used as controls. For the real-time PCR analysis, RNA isolation was first performed using a column-based RNA isolation kit (Nucleospin RNA isolation kit, Macherey Nagel, Düren, Germany), followed by reverse transcription by a superscript first-strand synthesis kit (Takara Bio USA Inc.), both according to the manufacturer's

instructions. Reactions were performed using SYBR-Select PCR Master Mix (Applied Biosystems, Foster City, CA) in a Step One Plus thermal cycler (Applied Biosystems). All reactions started with two initial incubation steps at 50 ˚C for 2 min for uracil-N-glycosylase (UNG) activation, and at 95 ˚C for 2 min for activation of the AmpliTaq DNA polymerase, and followed by 40 cycles of PCR, comprising denaturation for 15 s at 95˚C and annealing/extension for 1 min at 60 ˚C. Primers were designed using the PRIMER BLAST tool (https://www.ncbi.nlm.nih.gov/tools/primer-blast/). (Table S2). A standard melting curve was used to check the quality of amplification and specificity. The results were adjusted by amplification efficiency (LinRegPCR) and were normalized against two housekeeping genes, ACT-beta and GAPDH.

Antibacterial efficacy against *Enterococcus faecalis*

Bacterial strains and reagents. An *Enterococcus faecalis* strain previously isolated from poultry meat was used[23]. Cultures were performed in Brain Heart Infusion broth (BHI, CM1135, Oxoid Ltd.), Brain Heart Infusion agar (BHA, CM1136, Oxoid Ltd.), Tryptic Soy broth (TSB, LAB004, LabM) and Slanetz Bartley medium (CM00377, Oxoid Ltd.) at 37 ºC. The strains were revived

from glycerol stock cultures maintained at -80 ºC by aerobic culture at 37 ºC in BHI and verified for typical E. faecalis characteristics by standard morphological, biochemical, and antibiotic resistance characteristics. Decimal dilutions were performed in Maximum Recovery Diluent broth (MRD, T CM0733, Oxoid Ltd.) and surface platting was performed in either BHA or cation adjusted MH agar (B11438, Becton Dickinson).

***In Vitro* Assays**

Determination of the minimum inhibitory concentration (MIC), minimum bactericidal concentration (MBC), and minimum biofilm inhibitory concentration (MBIC). A micro-MIC method was used for the determination of the MIC according to the CLSI guidelines [24]. In brief, a fresh culture was prepared in BHI and incubated in an orbital shaking incubator at 37 ºC at 300 rpm (ISLD04HDG, Ohaus Ltd). The turbidity of the inoculum was adjusted to 0.5 McFarland by the use of a densitometer (Densimat, Biomerieux). The adjusted inoculum was further diluted 100-fold with sterile BHI in order to approximately achieve a $5*10^6$ CFU/mL concentration. The microbial count of the working inoculum was verified by surface platting in BHA and incubation at 37 ºC for 24-48 h. Ninety-six well sterile microplates were used. Two-fold dilutions of the films

under investigation dissolved in sterile BHI were prepared. In each well of the microplate, 100 μL of the film solution, 80 μL of sterile BHI and 20 μL of the diluted inoculum were placed. In each microplate a strip of wells was reserved as a negative control (substitution of the inoculum by sterile BHI) and another strip as positive control (substitution of the film solution by sterile BHI). The microplates were sealed to prevent evaporation and were incubated aerobically at 37 ^{o}C for 24 h. After incubation, the plates were examined macroscopically for bacterial growth. The visual results were verified by measurement of the absorbance at 630 nm with the use of an ELISA reader (DAS Italy). The last dilution inhibiting visual growth in BHI was recorded as the MIC. The MBC was measured by surface platting 10 μL from each well in BHA. After incubation at 37 ^{o}C for 24 h the inoculated petri dishes were examined for growth. The last dilution inhibiting growth in BHA was recorded as the MBC. Biofilm inhibition was performed according to the protocols of Li et al. (2020)[25] and Kwansy & Opperman (2010)[26]. In brief, an initial inoculum of $5*10^8$ CFU/mL was prepared as described above. The appropriate dilutions were made in Tryptic Soy Broth (TSB), supplemented with 1% glucose in order to achieve a final concentration of $5*10^6$ CFU/mL. The films were dissolved in 1% glucose TSB, supplemented with 1% glucose, at a final concentration of 300 μg/mL and two-fold dilutions were performed as previously described. The final volume in

each well was 200 μL and the plate was incubated at 37 ºC for 24h. After incubation, the optical density at 630 nm of each well was measured using a plate reader (DAS Italy), in order to quantify overall growth (biofilm and planktonic). Then, the planktonic cells were washed gently with normal saline in order to remove free cells without disrupting the biofilm. The plates were air – dried for ~1 h at 60 ºC and stained with the addition of 50 μL of 0.06% of crystal violet solution for at least 5 min at room temperature. Further, the wells were washed three times with normal saline. Solubilization of the stained crystal violet was performed with the addition of 200 μL of 33% acetic acid for 10 min at room temperature. The contents of the wells were transferred to a new microplate in which the absorbance was quantified using a plate reader (DAS Italy).

Time-Kill assay. For the estimation of the time kill kinetics of three representative film formulations (HPMC 3%-ZnO-Keto, CMC 3%- ZnO-Keto, PVA- ZnO-Keto), the method of Sim et al. (2014) was used with modifications[27]. In brief, an initial inoculum of 0.5 McFarland (approximately $5*10^8$ CFU/mL) was prepared. Triplicates of sterile tubes containing 5 mL of fresh sterile BHI (controls), or 0.5*MIC, 1*MIC, 2*MIC and 3*MIC film suspensions in BHI, were inoculated with 10 μL of the suspension in order to achieve an initial inoculum of 10^6 CFU/mL

further verified by surface platting, as previously described. The tubes were incubated in an orbital shaking incubator at 37 ºC at 300 rpm (ISLD04HDG, Ohaus Ltd). Samples were collected and examined for the bacterial counts after 1 h, 2 h, 4 h, 8 h and 24 h by decimal dilutions in MRD, plating in cation adjusted MH agar and incubation at 37 ºC for 24-48 h.

***Ex vivo* assay employing a human tooth culture model**. A total of 21 freshly extracted straight single-rooted human teeth were stored in formalin 10% for 2-3 weeks. The teeth were extracted for either periodontal or orthodontic reasons and were selected through random sampling from teeth with anatomically similar dimensions, with fully developed apices, without cracks or fractures. The study conformed to the ethical guidelines of the World Medical Association Declaration of Helsinki.

The specimens were decoronated to a standard root segment length of 14 mm using a diamond bur adjusted in high-speed handpiece under water irrigation. The root canal working lengths were determined by using a K-file size 15 (Densly, Maillefer, Switzerland) through the apical foramen. The root canals were prepared though crown-down technique, cleaned and shaped by using Ni-Ti rotary files under gold proprietary processing (Protaper Gold System, Densply, Maillefer,

Switzerland) with the following sequence: SX, Proglider Gold, S1, S2, F1, F2, F3, F4) under irrigation of 3 mL 2.5% w/v NaOCl after the use of each rotary instrument with a 30 G needle. Smear layer was removed by the use of 1 mL 17% EDTA left for 1 min, followed by final rinsing with 3 mL of 0.9 % sodium chloride solution. The specimens were autoclaved at 121 ^{o}C for 20 min. After sterilization, roots were incubated in sterile BHI to ensure no bacterial contamination. The excised roots were incubated with *E. faecalis* to establish a biofilm. A standard inoculum of $5*10^{8}$ CFU/mL was prepared. In a tube containing 3 mL of BHI, 100 µL of the inoculum were placed along with one excised tooth. After incubation for a week at 37 ^{o}C during which the tubes were inspected daily, the teeth were removed aseptically and dried gently with the use of sterile paper points. The roots were randomly categorized in seven different groups, including those treated with the different electrospun film formulations, as well as the positive and the negative control (3 roots/group, n=3). Following the washing steps, the respective treatment was applied on each of the groups. In the positive control group, irrigation by 5 mL of 2.5% w/v NaOCl was applied, whereas in the negative-control group, irrigation by 5 mL 0.9% of sodium chloride solution was applied. In the root groups exposed to the electrospun films, 15.1 mg ± 0.1 mg of each film were applied in the root canals with simultaneous irrigation with BIH-broth by means of

a sterile 30 G needle to enable the dilution of the films inside the root canal. After treatment, the teeth were placed individually in a sterile Eppendorf tube on top of 300 μL of fresh culture of $5*10^5$ CFU/mL E. faecalis, without covering the apical orifice of each root. The teeth were kept at 37 ºC for 24 h to simulate the *in vivo* conditions following dental interventions with the films under investigation. Further, samples were collected from the teeth root channels and the underlying BHI culture. Root channel sampling was performed with the use of three sterile dental points exercising excessive force. The points were vortexed and briefly (30 s) sonicated in 1 mL of MRD to suspend the collected bacteria. Similarly, 50 μL of the underlying culture were collected and added to 950 μL of MRD. Decimal dilutions were performed in MRD, then surface plated in BHA, and incubated at 37 ºC for 24-48 h. The first dilution of both the teeth and the underlying culture was surface platted in Slanetz Bartley medium to check for contamination by other microorganisms.

Imaging-based characterization of the *ex vivo* human tooth model. Imaging-based characterization was conducted employing X-ray micro-computed tomography (μCT) and Scanning Electron Microscopy. Briefly, μCT imaging was used to image the intact specimens prior to the destructive

preparation of SEM analysis, which required breaking open the teeth to expose the root canal. To avoid interfering with the samples, all samples were scanned in their original container, which was filled with formalin buffer solution. Imaging was conducted at ~ 85 kVp / 7 W using a reflection target at a voxel-size of 6.5 -8 μm depending on the field of view and the specimen size. During the 360° tomogram, 1500 -2000 projections were collected with 4-frames being averaged per projection to improve signal-to-noise ratio. Following acquisition, the data were reconstructed into 32-bit volume files using the manufacture's reconstruction software, which uses a filtered-back projection algorithm. The reconstructed 32-bit raw image volumes were then converted to 16-bit volumes for visualization, which was done using Volume Graphics VGStudioMax 2.1.4.

For the imaging experiments the following samples were used: 1x negative control (treated with 0.9% of sodium chloride solution); 1x positive control (treated with of 2.5% w/v NaOCl); 1x HPMC 3%-ZnO-Keto film-treated; 1x HPMC 1%-ZnO-Keto film-treated; 1x CMC 3%- ZnO-Keto film-treated; 1x CMC 1%-ZnO-Keto film-treated; 1x PVA- ZnO-Keto film-treated.

SEM imaging of the *ex vivo* human tooth model. Preparation for SEM imaging required breaking the teeth open to expose the root canal by carefully driving a sharp object (surgical blade) from

the side of the tooth and through the root canal, while keeping the sample hydrated. During this process the tooth was split along the length of canal. To preserve the structure of any biofilm that might had developed into the canal, the samples were carefully dried before sputtering using critical point drying. The process involves the slow exchange of the water with ethanol in steps of increasing ethanol to water solutions. When the sample was in 100% ethanol, the ethanol was replaced with liquid CO_2 using a CO_2 critical point dryer (Balzers CPD 030). Followingly, the samples were affixed onto 12.5 mm SEM stubs and coated with ~7 nm of Platinum (particle size ~7 nm; Quorum Q150T ES) and visualized by SEM using an FEI Quanta FEG 250 Scanning Electron Microscope.

Statistical analysis. Statistical analysis of the data employed two-way analysis of variance (ANOVA), while multiple comparisons between groups were analyzed with Tukey's post-hoc test using Prism 8.0 Software (GraphPad, CA, USA). All quantitative experiments were performed in at least triplicates and repeated at least three times. Data were expressed as means (± standard deviation; SD), and statistical significance was set at $p < 0.05$.

RESULTS

Characterization of the ZnO nanoparticles and nanofiber morphology. Figure 1A illustrates the X-ray diffractograms of the synthesized ZnO NPs and the JCPDS standard card No 36-1451, which corresponds to the wurtzitic structure of ZnO. All observed diffraction peaks are in coincidence with the wurtzite structure of ZnO and no other crystalline phase such as ($Zn(CH_3COO)_2 \cdot 2H_2O$) or $Zn(OH)_2$ was observed. A broadening of the diffraction peaks is also observed due to the low crystallite size. The average particle size of the nanocrystallites was calculated by the Scherrer formula[28], and in our case, the (002) reflection peak of ZnO was used to calculate the average particle size. The calculated mean size was 4.2 nm. A representative TEM image of ZnO NPs is shown in Figure 1B and the size distribution obtained from the TEM images is shown in the inset. The calculated mean size is at 4.5 ± 0.4 nm, which is in good agreement with the size calculated from the XRD pattern. The morphology and diameter distribution of the plain and Keto-ZnO loaded electrospun fibers were assessed by SEM (Figure 1). Plain nanofibers (Figure 1C-G) appeared to be smooth and uniform with random orientation. Electrospinning of the neat PVA solution resulted in ultrathin fibers with an average diameter of 197 nm ± 68 nm. The average diameter of the electrospun fibers increased with increasing the concentration of total solids (Figure 1c-g). Homogenous bead-free nanofibers were also obtained when solutions containing ketoprofen and ZnO NPs were electrospun (Figure 1H-L). Similar to the plain nanofibers, a notable

increase in the average fiber diameter was also observed for the Keto-ZnO loaded nanofibers with increasing the concentration of total solids (Figure 1h-l). TEM analysis was performed on a representative nanofiber formulation to verify the presence and localize the ZnO NPs in the nanofibers. As shown in Figure 2, ZnO NPs were found to be embedded within the polymer matrix of the HPMC 3%-Keto-ZnO nanofibers with an even distribution both in the core-center and the surface of the fibers. The TEM tilt series images viewed as a video further support this, as the different viewing angle allows for a more accurate interpretation the NPs' spatial distribution (Video S1).

Assessment of drug crystallinity with DSC and XRD analysis. The thermal properties of the raw materials, plain and Keto-ZnO loaded films were assessed with DSC analysis (Figure S1A-C). Crystalline ketoprofen showed a sharp endothermic peak at 97 ˚C, corresponding to its melting temperature (Tm), while PVA exhibited two minor endotherms, the first one at 60.8 ˚C, corresponding to its glass transition temperature (Tg) and the second at 192 ˚C, related to its melting point. No peak related to the Tm of ketoprofen was observed in the thermograms of the Keto-ZnO loaded films. The physical state of the drug in the electrospun films was investigated with XRD analysis (Figure S1D-F). The XRD patterns of crystalline ketoprofen showed sharp diffraction peaks at 6.22˚, 14.53˚, 18.57˚, 20.19˚, 22.72˚, 23.02˚, and 24.08˚ [29]. Both cellulose

derivatives demonstrated a broad halo in the 2θ range between 15˚ and 25˚, corresponding to their semi-crystalline nature, similar to PVA for which a single Bragg's reflection was observed at 2θ%=%19.4˚, corresponding to the (101) plane. The diffraction peaks of the ZnO NPs at 31.6˚, 34.6˚, 36.4˚, 48.1˚, and 56.4˚, correspond to the reflections from (100), (002), (101), (102), and (110) crystal planes of the ZnO structure [30]. No diffraction peaks corresponding to crystalline ketoprofen were identified in the XRD patterns of the Keto-ZnO loaded electrospun films (Figure S1F). In addition, the minor peaks detected at 34.6˚ and 36.4˚ confirmed the presence of the ZnO nanoparticles in the films.

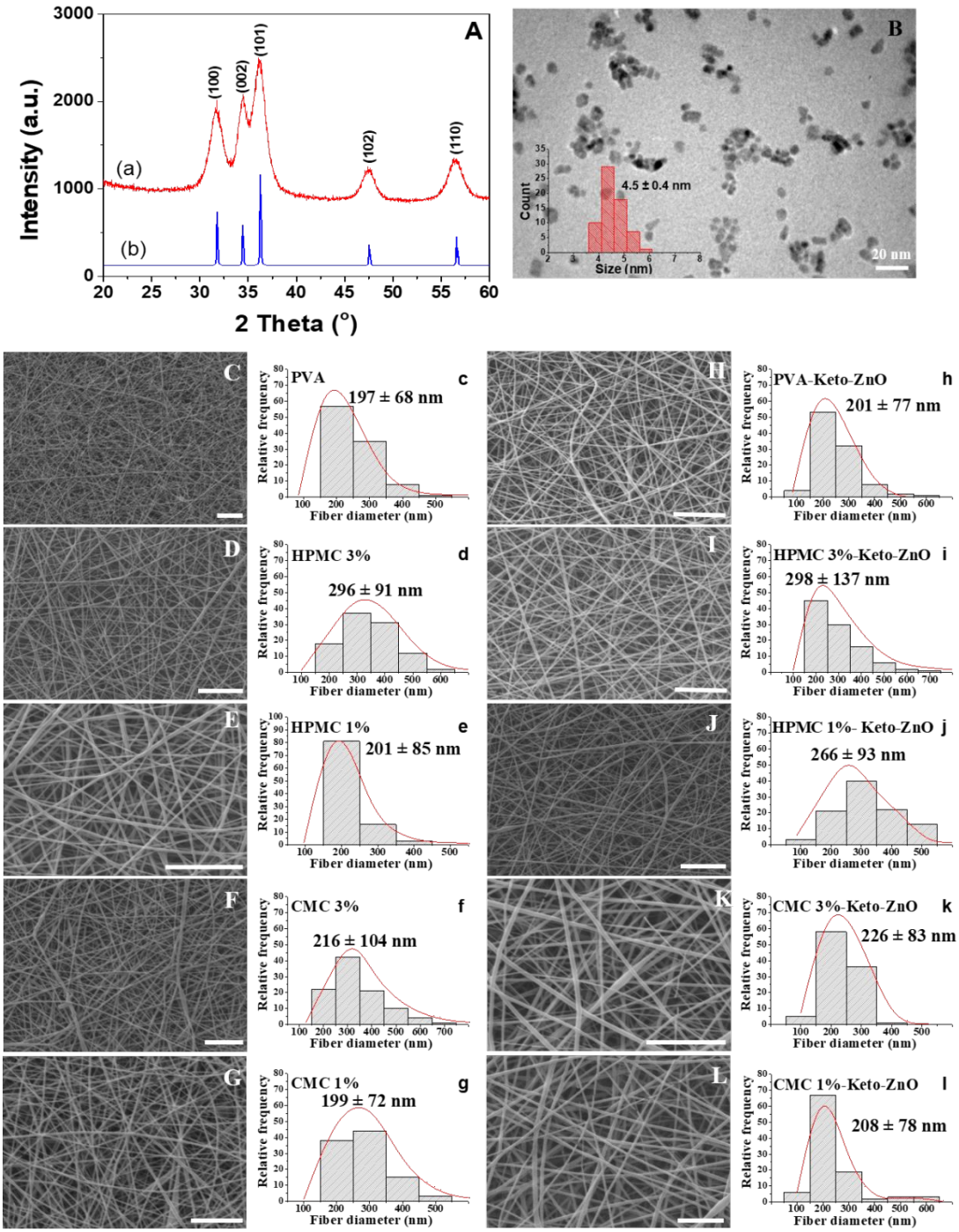

435

436 **Figure 1**. **A**. XRD graph of (a) synthesized ZnO nanoparticles and (b) JCPDS standard card No

437 36-1451 for ZnO. **B**. TEM image of the synthesized ZnO quantum dots. The inset represents the

438 particle size distribution graph. **C-L**. SEM images and c-l. fiber diameter distribution of C. PVA,

D. HPMC 3 %, E. HPMC 1%, F. CMC 3%, G. CMC 1%, H. PVA-Keto-ZnO, I. HPMC 3%-Keto-ZnO, J. HPMC 1%-Keto-ZnO, K. CMC 3%-Keto-ZnO, L. CMC 1%-Keto-ZnO. Scale bar: 1 μm.

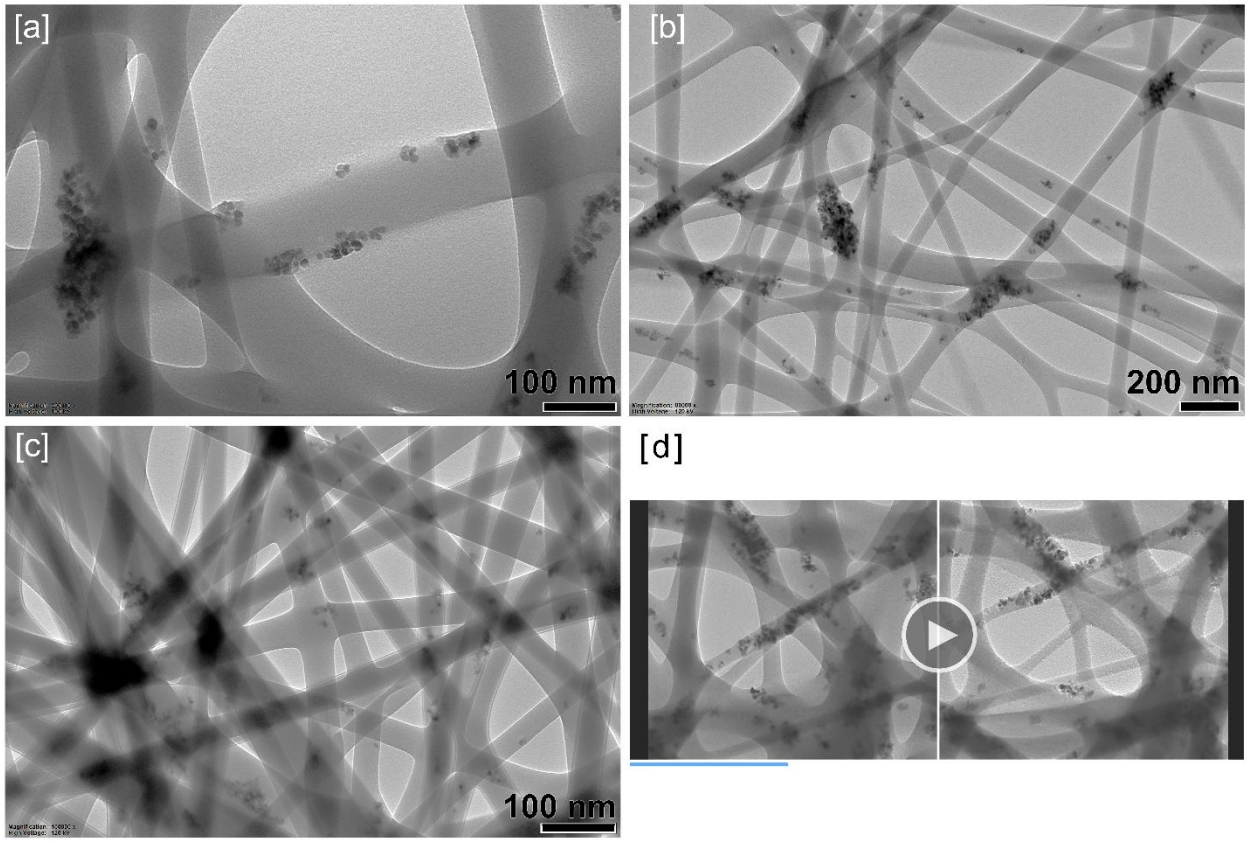

Figure 2. Representative TEM images of the HPMC 3%-Keto-ZnO electrospun nanofibers showing ZnO distribution within the fibers at different magnifications. The TEM tilt series images viewed as a video (thumbnail d) allow for a more accurate interpretation the NPs' spatial distribution (Video-S1).

***In vitro* disintegration time and *in vitro* drug release studies**. All films absorbed water rapidly upon contact with the wet paper, resulting in the formation of transparent gels. For the plain films, disintegration occurred within less than 20 s, in contrast to the Keto-ZnO loaded films which did not fully disintegrate even after 300s (Figure 3). This could be attributed to the hydrophobic nature of the ZnO NPs, which increase the hydrophobicity of the films [31]. The drug content in the Keto-ZnO films (16.6%-16.9%) was very close to the theoretical value (16.6%), therefore achieving almost 100% encapsulation efficiency. The *in vitro* ketoprofen release profiles from the Keto-ZnO films were recorded in SSF pH 6.8 at 37 ˚C in the presence of 0.5% v/v Tween 80 (Figure 4). A burst effect was observed for all formulations with *ca.* 20-30% of ketoprofen being released upon contact with SSF, and total drug release attained within 5 min.

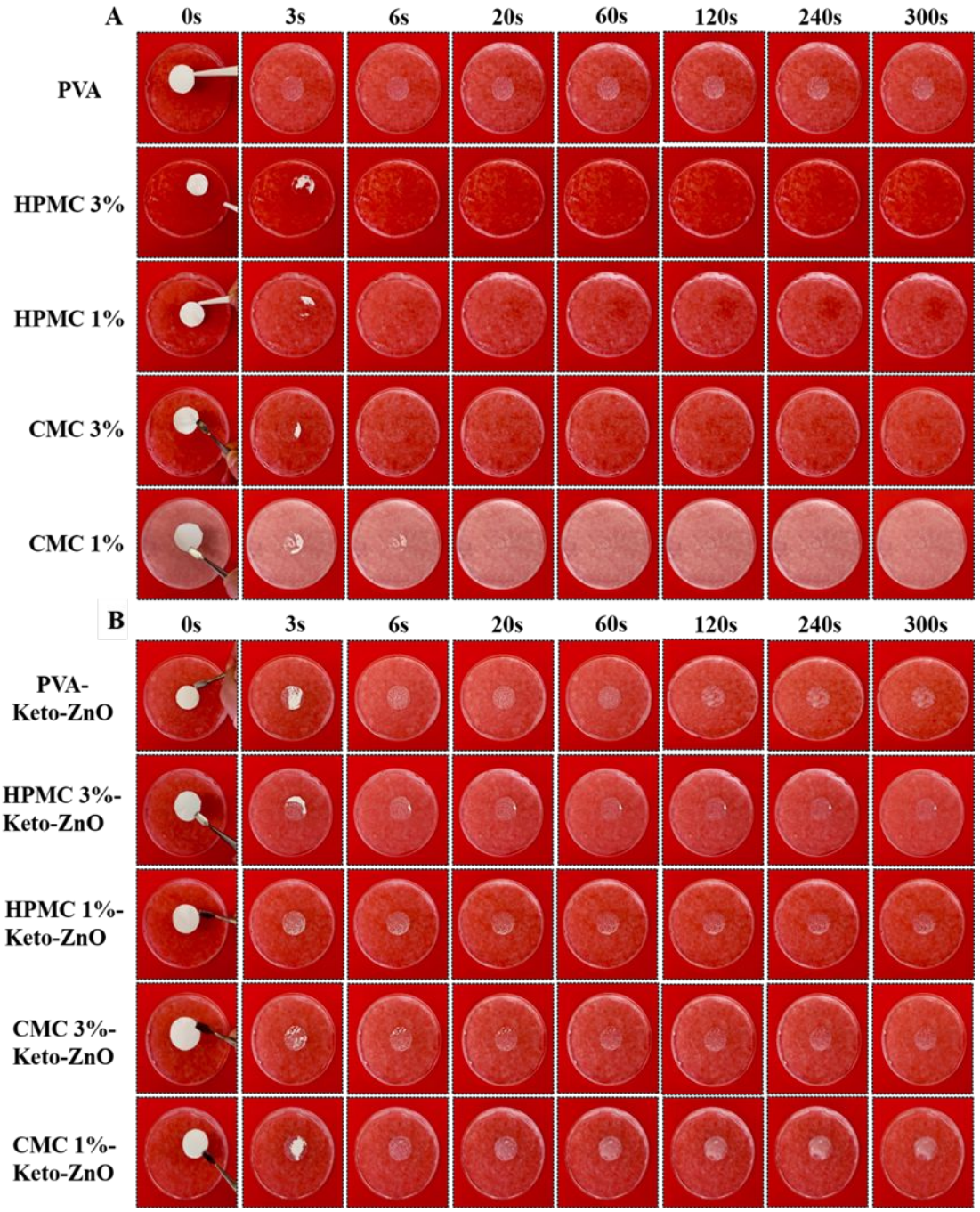

Figure 3. Estimation of the *in vitro* disintegration time of the **A.** plain and **B.** Keto-ZnO loaded electrospun films in simulated salivary fluid (pH 6.8).

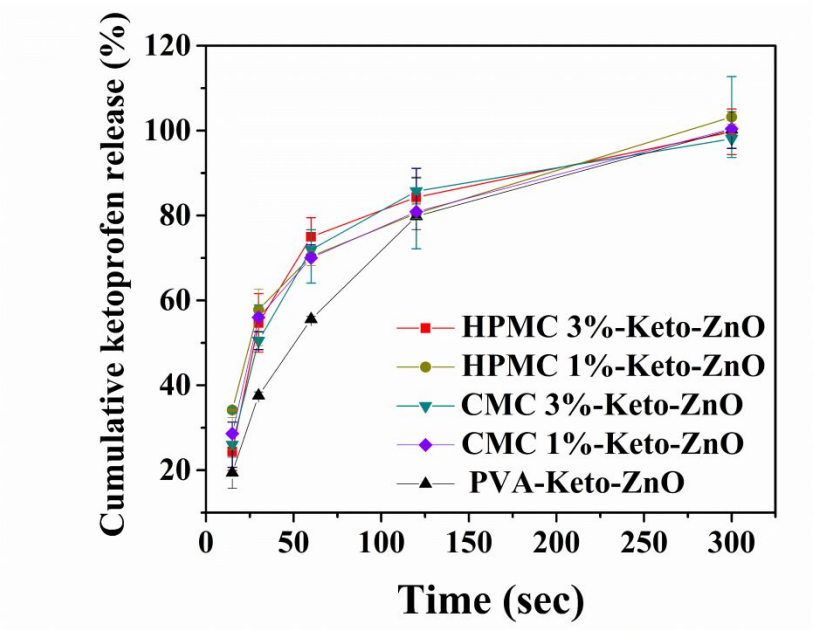

Figure 4. *In vitro* release profiles of ketoprofen from the Keto-ZnO loaded electrospun films in simulated salivary fluid pH 6.8 at 37 ºC in the presence of 0.5% v/v Tween 80.

MTT cell viability assay and gene expression analysis of pro-and anti-Inflammatory markers of RAW 264.7 Cells. The MTT cell viability results showed a reduction of RAW 264.7 cell viability exposed to the films containing the higher ketoprofen concentrations of 0.5 mg/mL and 1 mg/mL at all three-time points examined (Figure 5). In contrast, cell viability/proliferation ($p<0.001$) for almost all different films containing 0.1 mg/mL ketoprofen increased at 24 h. Overall, the films with the highest concentration of each cellulose derivative had slightly better cell viability performance than the films with the lowest concentration. Besides, the 3% CMC derivative showed

a better biological performance than the 3% HPMC derivative when combined with 1 mg/mL ketoprofen. Comparison between the electrospun fibers containing CMC 3% and the ones without any cellulose derivative showed a better biological performance of the CMC-based films for the three higher concentrations of ketoprofen used. Overall, there was a concentration-dependent impact of the ketoprofen in the films, with a decrease in viability at the highest concentrations (0.5- and 1 mg/mL), while achieving the highest cell viability/proliferation values at 0.1 mg/mL at 24 h.

This ketoprofen concentration (0.1 mg/mL) was selected for the further gene expression analysis of the pro-inflammatory cytokines MMP-3, MMP-9, MMP-13, MCP-1 and IL-6, and the anti-inflammatory marker IL-10. The present study results showed that application of PVA-Keto0.1-ZnO on LPS-stimulated RAW264.7 cells induced significant upregulation of pro-inflammatory genes compared with the control group at 24 h (Figure 6). In contrast, the films containing different concentrations of cellulose derivatives induced a significant downregulation of the pro-inflammatory genes while suppressing the transcription of IL-10. The HPMC 3%-Keto0.1-ZnO film induced the most pronounced effect in downregulating the expression of MCP-1, IL-6, and MMP-13 at both 24 h and 48 h ($p<0.001$), MMP-3 at 24 h ($p<0.001$), MMP-9 at 48 h ($p<0.001$)

and IL-10 ($p<0.05$ at 24 h and $p<0.001$ at 48 h). The fibers containing CMC at different concentrations induced variable results regarding their anti-inflammatory action. Both scaffolds stimulated the transcription of MMP-9 at 24 h ($p<0.001$), while reducing it at 48 h. CMC 3%-Keto0.1-ZnO had the same performance regarding MCP-1, increasing its expression at 24 h ($p<0.001$), while decreasing it at 48 h ($p<0.05$), but showed optative results in the downregulation of the rest of pro-inflammatory genes [MMP-13 at 24 h ($p<0.05$), MMP-13 at 48h ($p<0.001$) and IL-6 at 24 h ($p<0.05$) and 48 h ($p<0.001$)].

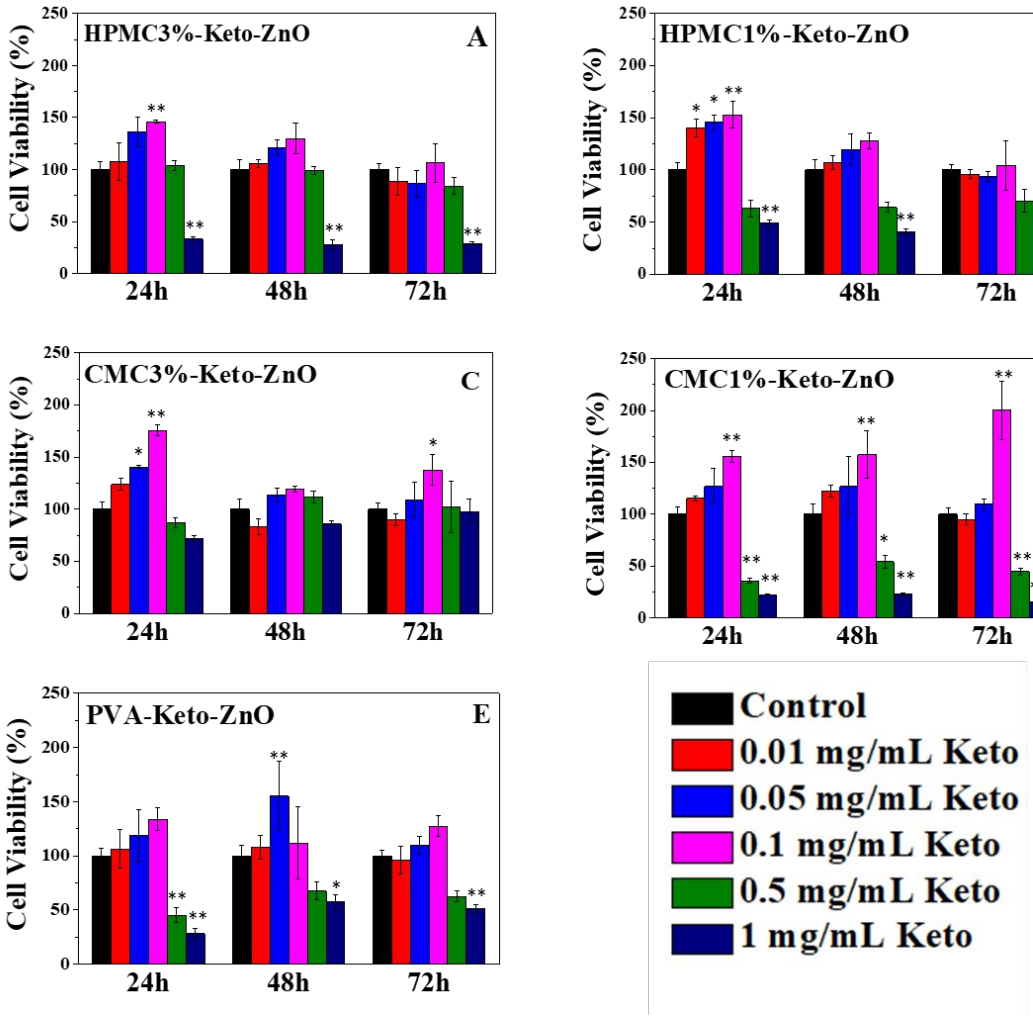

Figure 5. MTT cell viability assay of RAW 264.7 cells exposed to the electrospun films **A.** HPMC3%-Keto-ZnO, **B.** HPMC1%-Keto-ZnO, **C.** CMC3%-Keto-ZnO, **D.** CMC1%-Keto-ZnO and **E.** PVA-Keto-ZnO containing increasing ketoprofen concentrations (0.01-1 mg/mL) for 24 h, 48 h and 72 h.

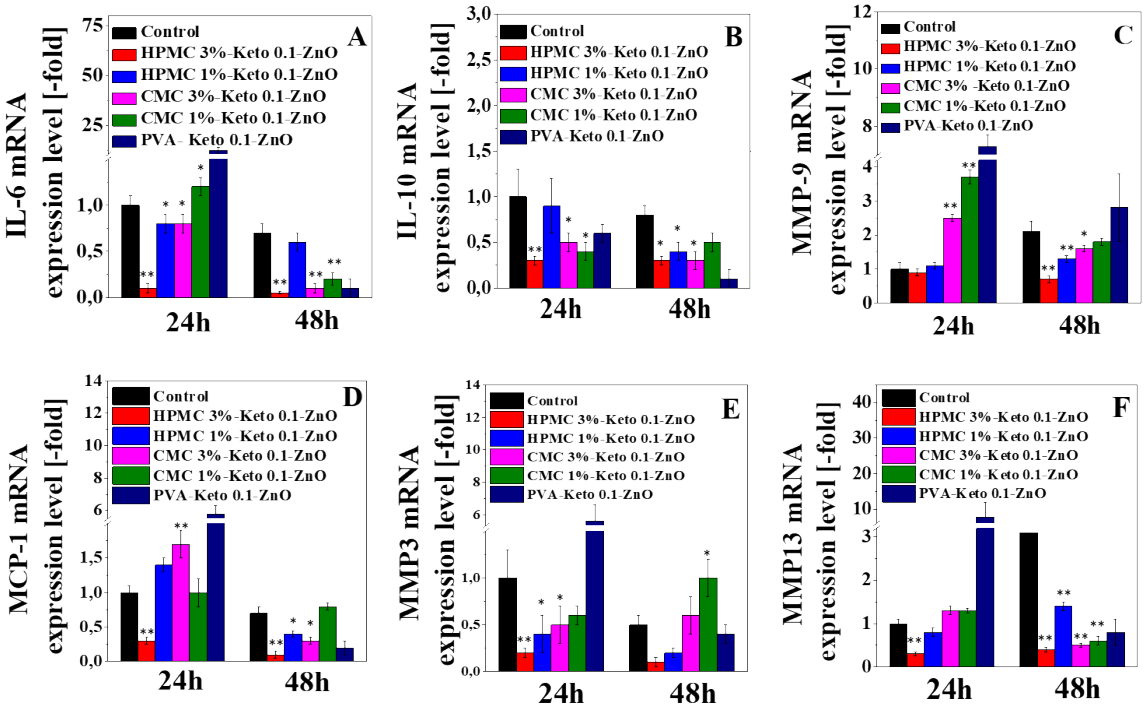

Figure 6. Gene expression analysis of pro- and anti-inflammatory markers **A.** IL-6, **B.** IL-10, **C.** MMP-9, **D.** MCP-1, **E.** MMP3 and **F.** MMP13 of RAW 264.7 cells exposed to the electrospun polymeric films containing ketoprofen at 0.1 mg/mL for 24 h and 48 h.

Antibacterial efficacy against *E. faecalis*

MIC, MBC, and MBIC assays. The MIC, MBC and MBIC values are shown in Table S3. All films exhibited a MIC of 75 µg/mL, whereas their MBC was 300 µg/mL. It was interesting though, that the MBIC values of the films were quite lower, with HPMC 3%-Keto-ZnO and HPMC 1%-Keto-ZnO having a MBIC of 0.29 µg/mL and CMC 3%- Keto-ZnO, CMC 1%-Keto-ZnO, and PVA-Keto-ZnO exhibiting a MBIC of 0.15 µg/mL.

Time-Kill kinetics. The time-kill kinetics of HPMC 3%-Keto-ZnO, CMC 3%-Keto-ZnO, and PVA-Keto-ZnO are shown in Figure S2. The 1*MIC (75 μg/mL) and 2*MIC (150 μg/mL) concentrations of the HPMC 3%-Keto-ZnO film showed an effect, with the 2*MIC concentration inducing a bacteriostatic effect. The CMC 3%-Keto-ZnO film showed a similar trend, with the 1*MIC concentration (75 μg/mL) and the 2*MIC concentration (150 μg/mL) showing inhibition of bacterial growth. The 3*MIC concentration (225 μg/mL) was characterized as bacteriostatic. The PVA-Keto-ZnO film 1*MIC (75 μg/mL) and 2*MIC (150 μg/mL) concentrations showed a similar trend to the CMC 3%- Keto-ZnO, with the 1*MIC concentration showing a temporary inhibitory effect and the 2*MIC concentration exhibiting inhibition. However, the 3*MIC concentration (225 μg/mL) of the PVA-Keto-ZnO formulation was bactericidal, resulting in no bacterial growth after 24 h.

***Ex vivo* studies.** The viable *E. faecalis* counts recorded during the *ex vivo* experiment are shown in Figure 7B. The viable counts from the root channels after treatment with all films were comparable to the ones after NaOCl application, which is considered the standard practice for root canal disinfection. The PVA-Keto-ZnO film showed a significantly higher bactericidal effect compared to the NaOCl treatment ($p<0.05$). The HPMC 3%-Keto-ZnO and HPMC 1%-Keto-ZnO films showed a trend for lower *E. faecalis* counts compared to NaOCl, failing, however, to reach statistical significance ($p>0.05$). The effect of HPMC 3%-Keto-ZnO, HPMC 1%-Keto-ZnO, CMC 3%-Keto-ZnO and CMC 1%-Keto-ZnO films on the underlying broth culture was minor, whereas the effect of the PVA-Keto-ZnO film was comparable to that of NaOCl.

Imaging-based characterization of the *ex vivo* human tooth model. Imaging with μCT allowed for root-canal inspection prior to destructive testing, and the volume images serve as an archive of the sample's geometry for future reference. After treatment, the canal appeared empty in its entity, although in some cases, film residues were observed towards the lower part of the canal (Figure 7A, HPMC 1%-ZnO-Keto film-treated). No biofilm was visible in the μCT volume images. The μCT images of all treated tooth samples are shown in Figure S3. SEM imaging confirmed the presence of both biofilm and bacteria in the negative control (Figure 7C). The biofilm appears dense and populated by bacteria, covering the dental matrix and intruding the dentinal tubules. The bacteria show the characteristic structure of *E. faecalis* and appear to be present both on the surface and within the biofilm. The positive control, on the other hand (Figure 7D/a-d), is free of biofilm with clean dentinal tubules, and no bacteria were observed in the exposed root canal. The treated samples showed an intermediate morphology (Figure 7E/a-d and Figure S4). Bright areas similar to the biofilm ones in the negative control samples were observed, nevertheless, at higher magnification, these areas were identified as nanofiber film residues coating the surface of the canal, since they were much less-dense, patchy, and consisting of a dense network of fibrils. It is possible that some biofilm was also present at some point, however the treatment most likely affected the amount of biofilm deposited by controlling the viability of the bacterial population. Similar to the positive control, no bacteria were observed in the exposed root canal or the film residue areas.

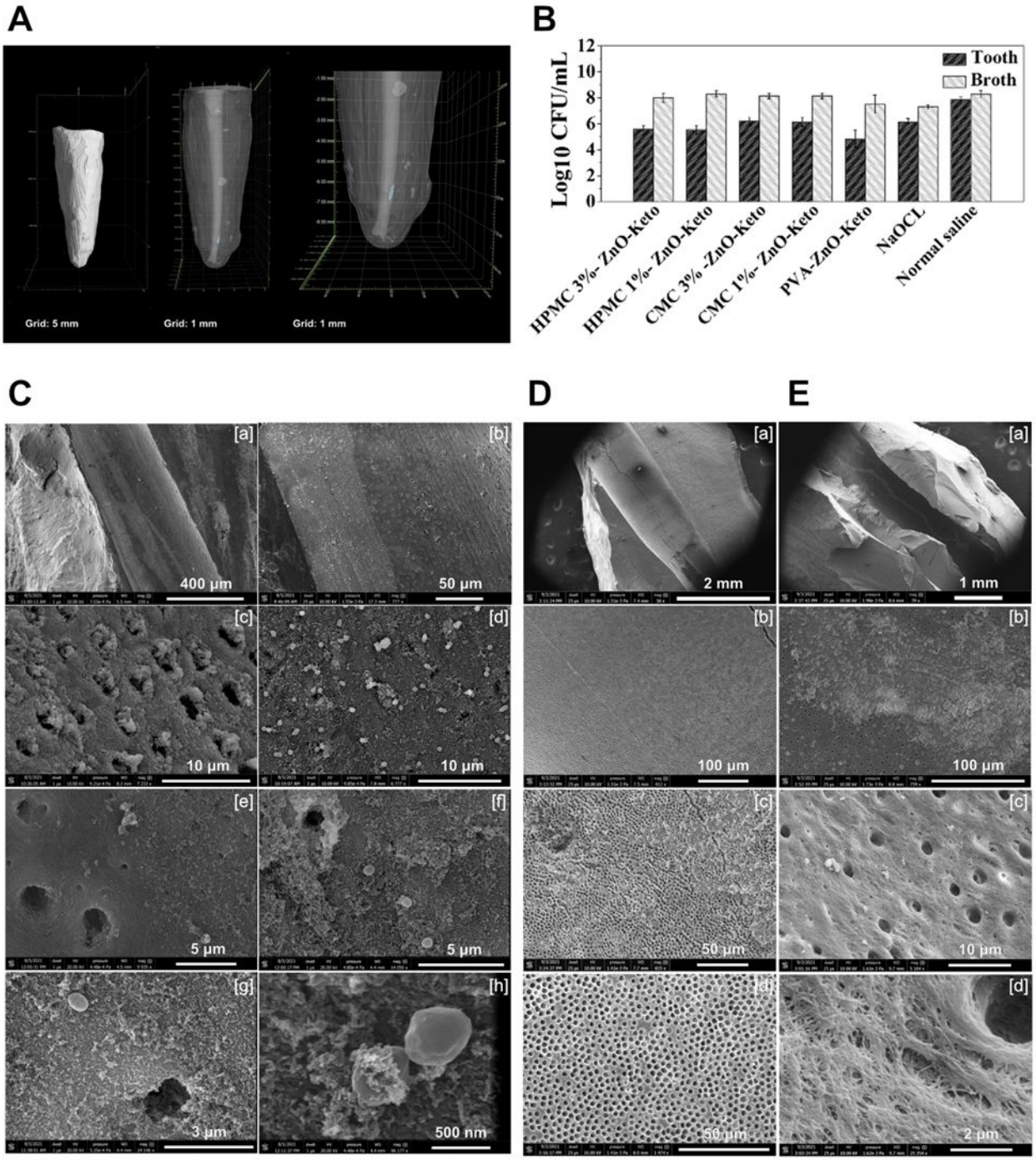

Figure 7. A. Opaque and semi-transparent volumetric rendering of human tooth showing residue of the film (middle- and right panel; pseudocoloured blue). **B.** *E. faecalis* counts in the root canal and the underlying broth after the *ex vivo* application of the films. **C.** Negative control at different magnifications. **a.** Exposed root canal in the centre of field of view showing the bright biofilm

areas. Fracture areas are also visible at this magnification on either-sides of the image; **b.** Image focusing on the exposed root canal. Bacterial population appears as small bright dots across the canal surface; **c.** Thick biofilm development and intrusion into the dentinal tubules; **d.** Thick biofilm with individual bacteria spread across it; **e**. transition zone from biofilm-free to biofilm containing an area of the canal; **f -h.** Higher magnification images of biofilm structure, bacteria, and single dentinal tubule for comparison. **D. a -d**: Positive control at different magnifications. Canal surface appears free of biofilm with clean dentinal tubules, although some unidentified sparce residue can be seen in some areas. No bacteria could be seen anywhere in the exposed root canal. **E. a -d:** PVA-Keto-ZnO film treated tooth sample at different magnifications. Bright areas shown in the low-magnification image consist of a dense network of fibers corresponding to the PVA-Keto-ZnO film. These areas are much less-dense, patchy and in some areas consisting of a dense network of fibrils.

DISCUSSION

Successful management of endodontic infections is essential to avoid persistent periapical infections following root canal treatment. Irrigation with NaOCl is the "gold standard" for clinical root canal disinfection; however, its unpleasant odor, high toxicity, and high potency of provoking allergic reactions has driven research interest in alternative nanomaterial-based therapeutic approaches to address the anti-inflammatory, antimicrobial, as well as postoperative pain relief requirements of root canal treatment. In this work, we aimed to address the shortcomings of current treatment approaches, stemming from the anatomical restrictions of the root canal space, by fabricating a hydrophilic electrospun nanofiber film for the local co-administration of an antimicrobial (ZnO NPs) and an anti-inflammatory (ketoprofen) agent. Rapid disintegration of the

films occurred within seconds upon contact with aqueous media to constitute both active agents readily available at the site of action. This is highly desirable to mitigate the side effects commonly associated with the non-specific distribution of orally administered non-steroidal anti-inflammatory drugs in the treatment of post-operative pain and inflammation[32]. In addition, drug amorphization, confirmed by both DSC and XRD findings, combined with the increased nanofiber surface area available for drug release were the determinant factors contributing to the significant dissolution enhancement of the poorly water soluble ketoprofen from the electrospun films.

Ketoprofen has been widely used as an anti-inflammatory agent incorporated in electrospun drug delivery systems. When examined in terms of cell viability in other eukaryotic cell types, such as fibroblasts, it has been shown that it does not substantially affect cell viability, which is indicative of a good biocompatibility[33,34]. Li *et al.* (2017) combined ketoprofen with electrospun fibers blend of ethyl cellulose (EC) and poly [di (ethylene glycol) methyl ether methacrylate] PDEGMA at a standard drug-to-polymer ratio of 1:5 (w/w)[33]. Results showed that L929 fibroblast cell viability after exposure to all different electrospun compositions remained close to their negative control, without any statistical significance. In other experiments, Li *et al.* (2018) combined the thermosensitive polymer poly(N-isopropylacrylamide) (PNIPAAm) co-dissolved with the pH-sensitive polymer Eudragit (EL100-55) into fibers utilizing electrospinning incorporating ketoprofen as model drug. They performed the MTT assay to examine the cytotoxicity of three different electrospun fibers (PNIPAAm, EL100-55 and PNIPAAm/EL100-55) at three different concentrations each (100 mg/L, 50 mg/L, 25 mg/L), all of them loaded with 4% (w/v) ketoprofen on L929 fibroblasts. Results showed no statistically significant decrease in cell viability in none of the three different concentrations of fibers at 24 h compared to the control of untreated cells[34]. These results are indicative of acceptable biocompatibility of different polymers prepared via

electrospinning and containing ketoprofen at relatively low concentrations, come in accordance with the results of the present study.

The effect of ketoprofen in the current study reflects that the electrospun fibers present acceptable biocompatibility and could be suitable for several oral applications, requiring the presence of a local anti-inflammatory agent releasing system. LPS induction has served as an *in vitro* model of immune response stimulation in combination with many different cell types, especially with blood monocytes and tissue macrophages, responsible for the onset of inflammation[35]. While identification of the transcriptional profiling of tissue-resident macrophages presents extreme diversity and heterogeneity regarding tissue-specific functions during development and adulthood[36], the *in vitro* macrophage assay applied in this study represents a widely used valid tool for the assessment of anti-inflammatory activity[37].

Regarding the genes under investigation, MMPs are a family of endoproteases with a broad spectrum of action in tissue remodeling, and degradation of multiple components of the extracellular matrix (ECM)[38,39,40]. They affect a variety of bioactive molecules in cellular surfaces and modulate signaling pathways, therefore they play a fundamental role in leukocyte infiltration and tissue inflammation[38,41]. Various MMPs, including MMP-3 MMP-9 and MMP-13, are involved in the pathogenesis related to endodontic lesions and periapical tissue destruction and their presence constitutes an important factor for the progression and persistence of inflammation[39,40]. MCP-1 belongs to the family of chemokines which are secreted in response to signals related to inflammation and are responsible for selectively recruiting monocytes, neutrophils and lymphocytes. Chemokine MCP-1 has been detected in the periapical fluid of human root canal infections in recent studies[42]. IL-6 constitutes a pro-inflammatory cytokine present in multiple diseases[43]and IL-10 is a potent inflammatory cytokine with a key role in

preventing inflammation and autoimmune pathologies[44]. Both of them have been detected in high ratios in apical periodontitis in the course of an endodontic infection due to the action of Gram-negative bacteria virulence factors presented [39,45,46]. Therefore all the cytokine examined have been thoroughly selected since they are all present in apical periodontitis.

Comparing the overall effectiveness of downregulating pro-inflammatory and maintaining or upregulating anti-inflammatory factors among the different formulations, the conclusions favor HPMC 3%-Keto0.1-ZnO and CMC 3%-Keto0.1-ZnO. The first one had more effective results in downregulating most pro-inflammatory markers, exhibiting the most distinct anti-inflammatory performance amongst all different formulations, therefore showing promising therapeutic potential.

In the current study, the ability of ZnO-loaded electrospun films to inhibit bacterial proliferation and eradicate biofilm formation was investigated and verified both *in vitro* and *ex vivo* in an experimentally infected with *E. faecalis* human tooth culture model. *E. faecalis* is a Gram (+) anaerobic microbe present in periradicular infections. Given that it is the most frequent species present in post-treatment disease, it plays a crucial role in persistent periapical infections following root canal treatment[47]. It appears in both primary and secondary endodontic lesions and is often linked to endodontic failure, and therefore it is important to eradicate the infection to promote healing. Referring to the use of ZnO nanoparticles as antimicrobial agent, there are studies that have examined metallic NPs on their bactericidal effect in root canal irrigation. Luna *et al.*[48] developed an *ex vivo* root canal model contaminated with *E. faecalis* and examined the efficacy of silver NPs (537 mg/mL) irrigation compared to silver NPs with 17% EDTA, NaOCl and negative control by turbidity of the bacterial samples taken from the root canals. The silver NPs solution significantly eliminated the bacterial culture. NaOCl irrigation proved to be slightly more efficient

but not statistically significant compared to the effect of silver NPs. Silver NPs irrigation also achieved removal of smear layer according to Atomic Force Microscopy findings, compared to the action of EDTA and saline solution. The antimicrobial potency of ZnO NPs has been previously verified against both Gram (+) and Gram (-)[49]. In a study assessing *E. faecalis* biofilm structure after ZnO treatment, a significant reduction in the distribution of viable bacteria was observed after ZnO treatment for 24 h[50], while in an attempt to amplify the antibacterial action of commercialized root canal filling materials, gutta-percha (GP) points were coated with ZnO NPs showing significant inhibition in the viability of both *E. faecalis* and *S. aureus*[51]. The *in vitro* results of the current study demonstrate the antimicrobial and antibiofilm efficacy of Keto-ZnO loaded electrospun films against *E. faecalis* highlighting their clinical potential in antimicrobial endodontic treatment. *In vitro* findings were further corroborated by the *ex vivo* root canal model of bacterial contamination, a well-established model for antimicrobial endodontic tests[52]. The *ex vivo* model stimulates better the *in vivo* conditions with reference to a bactericidally infected root canal providing with an artificial environment for this purpose compared to an *in vitro* model with easier accessibility and less complexity than the *in vivo* stimuli[53]. Intracanal administration of the nanofiber films resulted in comparable post-treatment intracanal and periradicular CFU values to the ones obtained after NaOCl irrigation. Moreover, there has been shown that there are many cases up to 60% where positive bacterial cultures can still arise even after chemo-mechanical preparation with different NaOCl concentrations in cases of apical periodontitis[54,55]. This fact could come to terms with the limited decrease in *E. faecalis* culture within the root canal of our *ex vivo* experiment of NaOCl action compared to the negative control in 24 h sampling. SEM visualization of the treated root canals further confirmed the antimicrobial potency of the films,

which were deposited on the root canal surface, forming a hostile environment for bacterial growth and proliferation.

Electrospun nanofiber films loaded with pharmaceutical agents have been applied as drug delivery systems to eradicate bacterial infections in endodontic treatment. Karczewski *et al.* developed polydioxanone electrospun nanofibers containing a clindamycin-modified triple antibiotic to achieve bacterial elimination in cases of immature permanent teeth pulpal necrosis [12]. Porter *et al.* developed 3D tubular-shaped electrospun nanofibers containing either minocycline or doxycycline to examine tooth discoloration against different TAP systems in an *ex vivo* model of human canines[56]. Furthermore, Albuquerque *et al*.[11] aimed to investigate the antimicrobial action of 3-dimensional (3D) tubular-shaped triple antibiotic-eluting nanofibrous constructs against a multispecies biofilm on human dentin. Yet, to our knowledge, there is no report so far on a single solid dosage form that fulfills the antimicrobial, anti-inflammatory, and post-operative pain relief requirements for root canal treatment. Further investigation should focus on the *in vivo* efficacy of the proposed in the current study electrospun drug delivery system for the treatment of periradicular infections and endodontic lesions.

CONCLUSIONS

In the current study, polymeric fast-disintegrating films were successfully developed to address the antimicrobial and anti-inflammatory requirements for root canal treatment. The electrospun films showed good *in vitro* anti-inflammatory action on LPS-stimulated RAW 264.7 cells and adequate antimicrobial efficacy against *E. faecalis*, one of the most frequent species present in post-treatment disease. The antimicrobial efficacy of the nanofiber films was verified not only *in vitro* but also *ex vivo* in a human tooth model experimentally infected with *E. faecalis*. The

combination of anti-inflammatory and antimicrobial activity to be exerted directly at the site of action shows a very appealing application for the treatment of periradicular infections and endodontic lesions.

ASSOSIATED CONTENT: Composition of the spinning solutions, primers designed for the Real-time PCR analysis, MIC, MBC and MBIC values against *E. faecalis*, thermograms and X-ray diffractograms of the films, time-kill kinetics of the films against *E. faecalis* and μ-CT and SEM images of the root canals.

AUTHOR INFORMATION

Corresponding Author

Prof. Dimitrios Fatouros, e-mail: dfatouro@pharm.auth.gr

Author Contributions

The manuscript was written through contributions of all authors. All authors have given approval to the final version of the manuscript.

Funding Sources

Part of this work was supported by the Wellcome Trust Biomedical Resource and Technology Development Grant 212940/Z/18/Z and the National Research Facility for Lab X-ray CT (NXCT) through EPSRC grant EP/T02593X/1.

.

ACKNOWLEDGMENT

The authors acknowledge the μ-VIS X-ray Imaging Centre / X-ray histology facility and the Biomedical Imaging Unit (BIU) at the University of Southampton for the provision of μCT and SEM imaging facilities, data processing and management infrastructure and expertise. In addition, we would like to thank Patricia Goggin, Regan Doherty, and Catherine Griffiths at the BIU for their invaluable support. The graphical abstract has been designed using resources from Freepik.com. The authors also thank Dr. Maria Kollia of the Laboratory of Electron Microscopy and Microanalysis, School of Natural Sciences, University of Patras, Greece for the TEM images. The graphical abstract has been created with BioRender.com

References

(1) Siqueira, Jr. J. F. Endodontic Infections: Concepts, Paradigms, and Perspectives. Oral Surgery, Oral Med. Oral Pathol. Oral Radiol. Endod. 2002, 94 (3), 281–293. https://doi.org/10.1067/moe.2002.126163.

(2) Abusrewil, S.; Alshanta, O. A.; Albashaireh, K.; Alqahtani, S.; Nile, C. J.; Scott, J. A.; McLean, W. Detection, Treatment and Prevention of Endodontic Biofilm Infections: What's New in 2020? Crit. Rev. Microbiol. 2020, 46 (2), 194–212. https://doi.org/10.1080/1040841X.2020.1739622.

(3) Zehnder, M.; Belibasakis, G. N. On the Dynamics of Root Canal Infections—What We Understand and What We Don't. Virulence 2015, 6 (3), 216–222. https://doi.org/10.4161/21505594.2014.984567.

(4) Vijayaraghavan, R.; Mathian, V. M.; Sundaram, A. M.; Karunakaran, R.; Vinodh, S. Triple Antibiotic Paste in Root Canal Therapy. J. Pharm. Bioallied Sci. 2012, 4 (Suppl 2), S230–S233. https://doi.org/10.4103/0975-7406.100214.

(5) Montero-Miralles, P.; Martín-González, J.; Alonso-Ezpeleta, O.; Jiménez-Sánchez, M. C.; Velasco-Ortega, E.; Segura-Egea, J. J. Effectiveness and Clinical Implications of the Use of Topical Antibiotics in Regenerative Endodontic Procedures: A Review. Int. Endod. J. 2018, 51 (9), 981–988. https://doi.org/https://doi.org/10.1111/iej.12913.

(6) Wong, J.; Zou, T.; Lee, A. H. C.; Zhang, C. The Potential Translational Applications of Nanoparticles in Endodontics. Int. J. Nanomedicine 2021, 16, 2087–2106. https://doi.org/10.2147/IJN.S293518.

(7) Urquhart, E. Analgesic Agents and Strategies in the Dental Pain Model. J. Dent. 1994, 22 (6), 336–341. https://doi.org/https://doi.org/10.1016/0300-5712(94)90084-1.

(8) Naskar, S.; Chandan, Baskaran D.; Roy Choudhury, A.N.; Chatterjee, S.; Karunakaran, S.; Murthy, B.; & Basu, B. Dosimetry of pulsed magnetic field towards attaining bacteriostatic effect on Enterococcus faecalis: Implications for endodontic therapy. International Endodontic Journal. 2021, 54 (10), 1878– 1891. https://doi.org/10.1111/iej.13580

(9) Seo, S.-J.; Kim, H.-W.; Lee, J.-H. Electrospun Nanofibers Applications in Dentistry. J. Nanomater. 2016, https://doi.org/10.1155/2016/5931946.

(10) Pankajakshan, D.; Albuquerque, M. T. P.; Evans, J. D.; Kamocka, M. M.; Gregory, R. L.; Bottino, M. C. Triple Antibiotic Polymer Nanofibers for Intracanal Drug Delivery: Effects on Dual Species Biofilm and Cell Function. J. Endod. 2016, 42 (10), 1490–1495. https://doi.org/10.1016/j.joen.2016.07.019.

(11) Albuquerque, M. T. P.; Nagata, J.; Bottino, M. C. Antimicrobial Efficacy of Triple Antibiotic Eluting Polymer Nanofibers against Multispecies Biofilm. J. Endod. 2017, 43 (9), S51–S56. https://doi.org/10.1016/j.joen.2017.06.009.

(12) Karczewski, A.; Feitosa, S. A.; Hamer, E. I.; Pankajakshan, D.; Gregory, R. L.; Spolnik, K. J.; Bottino, M. C. Clindamycin-Modified Triple Antibiotic Nanofibers: A Stain-Free Antimicrobial Intracanal Drug Delivery System. J. Endod. 2018, 44 (1), 155–162. https://doi.org/10.1016/j.joen.2017.08.024.

(13) Sotomil, J. M.; Münchow, E. A.; Pankajakshan, D.; Spolnik, K. J.; Ferreira, J. A.; Gregory, R. L.; Bottino, M. C. Curcumin-A Natural Medicament for Root Canal Disinfection: Effects of Irrigation, Drug Release, and Photoactivation. J. Endod. 2019, 45 (11), 1371–1377. https://doi.org/10.1016/j.joen.2019.08.004.

(14) Kalyan, K. S. D. R.; Vinay, C.; Uloopi, K. S.; Chandrasekhar, R.; RojaRamya, K. S. Preclinical Evaluation and Clinical Trial of Chlorhexidine Polymer Scaffold for Vital Pulp Therapy. J. Clin. Pediatr. Dent. 2019, 43 (2), 109–115. https://doi.org/10.17796/1053-4625-43.2.7.

(15) Münchow, E. A.; Albuquerque, M. T. P.; Zero, B.; Kamocki, K.; Piva, E.; Gregory, R. L.; Bottino, M. C. Development and Characterization of Novel ZnO-Loaded Electrospun Membranes for Periodontal Regeneration. Dent. Mater. 2015, 31 (9), 1038–1051. https://doi.org/10.1016/j.dental.2015.06.004.

(16) Shao, J.; Yu, N.; Kolwijck, E.; Wang, B.; Tan, K. W.; Jansen, J. A.; Walboomers, X. F.; Yang, F. Biological Evaluation of Silver Nanoparticles Incorporated into Chitosan-Based Membranes. Nanomedicine 2017, 12 (22), 2771–2785. https://doi.org/10.2217/nnm-2017-0172.

(17) Nashaat, Y.; Sabry, H.; Hassan, S. A. Evaluation of the Cytotoxicity and Apoptotic Effect of Nano Triple Antibiotic Paste with Nano Anti-Inflammatory Drug as an Intracanal Medicament. Eur. Endod. J. 2021, 6 (1), 82–89. https://doi.org/10.14744/eej.2020.29292.

(18) Gaaz, T. S.; Sulong, A. B.; Akhtar, M. N.; Kadhum, A. A. H.; Mohamad, A. B.; Al-Amiery, A. A. Properties and Applications of Polyvinyl Alcohol, Halloysite Nanotubes and Their Nanocomposites. Molecules 2015, 20 (12), 22833–22847. https://doi.org/10.3390/molecules201219884.

(19) Siepmann, J.; Peppas, N. A. Modeling of Drug Release from Delivery Systems Based on Hydroxypropyl Methylcellulose (HPMC). Adv. Drug Deliv. Rev. 2001, 48 (2), 139–157. https://doi.org/https://doi.org/10.1016/S0169-409X(01)00112-0.

(20) Arca, H. C.; Mosquera-Giraldo, L. I.; Bi, V.; Xu, D.; Taylor, L. S.; Edgar, K. J. Pharmaceutical Applications of Cellulose Ethers and Cellulose Ether Esters. Biomacromolecules 2018, 19 (7), 2351–2376. https://doi.org/10.1021/acs.biomac.8b00517.

(21) Chachlioutaki, K.; Tzimtzimis, E. K.; Tzetzis, D.; Chang, M.-W.; Ahmad, Z.; Karavasili, C.; Fatouros, D. G. Electrospun Orodispersible Films of Isoniazid for Pediatric Tuberculosis Treatment. Pharmaceutics 2020, 12 (5), 470. https://doi.org/10.3390/pharmaceutics12050470.

(22) Marques, M. R. C.; Loebenberg, R.; Almukainzi, M. Simulated Biological Fluids with Possible Application in Dissolution Testing. Dissolution Technol. 2011, 18 (3), 15–28. https://doi.org/10.14227/DT180311P15

(23) Gousia, P.; Economou, V.; Bozidis, P.; Papadopoulou, C. Vancomycin-Resistance Phenotypes, Vancomycin-Resistance Genes, and Resistance to Antibiotics of Enterococci

806 Isolated from Food of Animal Origin. Foodborne Pathog. Dis. 2015, 12 (3), 214–220.
807 https://doi.org/10.1089/fpd.2014.1832.
808 (24) Weinstein, M. P.; Lewis II, J. S.; M, B. A.; Shelley, C.; Cullen, S. K.; Galas, M. F.; Gold,
809 H.; Humphries, R. M. CLSI M100-ED29 : 2019 Performance Standards for Antimicrobial
810 Susceptibility Testing , 29th Edition; 2019.
811 (25) Li, Y.; Wang, Y.; Chen, X.; Jiang, W.; Jiang, X.; Zeng, Y.; Li, X.; Feng, Z.; Luo, J.; Zhang,
812 L. Antimicrobial Peptide GH12 as Root Canal Irrigant Inhibits Biofilm and Virulence of
813 Enterococcus Faecalis. Int. Endod. J. 2020, 53 (7), 948–961.
814 https://doi.org/https://doi.org/10.1111/iej.13296.
815 (26) Kwasny, S. M.; Opperman, T. J. Static Biofilm Cultures of Gram Positive. Curr. Protoc.
816 Pharmacol. 2010, 1–27. https://doi.org/10.1002/0471141755.ph13a08s50.Static.
817 (27) Sim, J.-H.; Jamaludin, N. S.; Khoo, C.-H.; Cheah, Y.-K.; Halim, S. N. B. A.; Seng, H.-L.;
818 Tiekink, E. R. T. In Vitro Antibacterial and Time-Kill Evaluation of Phosphanegold(I)
819 Dithiocarbamates, R3PAu[S2CN(IPr)CH2CH2OH] for R = Ph, Cy and Et, against a Broad
820 Range of Gram-Positive and Gram-Negative Bacteria. Gold Bull. 2014, 47 (4), 225–236.
821 https://doi.org/10.1007/s13404-014-0144-y.
822 (28) Jensen, H.; Pedersen, J. H.; J∅rgensen, J. E.; Pedersen, J. S.; Joensen, K. D.; Iversen, S.
823 B.; S∅gaard, E. G. Determination of Size Distributions in Nanosized Powders by TEM,
824 XRD, and SAXS. J. Exp. Nanosci. 2006, 1 (3), 355–373.
825 https://doi.org/10.1080/17458080600752482.
826 (29) Yu, D.-G.; Yu, J.-H.; Chen, L.; Williams, G. R.; Wang, X. Modified Coaxial
827 Electrospinning for the Preparation of High-Quality Ketoprofen-Loaded Cellulose Acetate

828 Nanofibers. Carbohydr. Polym. 2012, 90 (2), 1016–1023.
829 https://doi.org/https://doi.org/10.1016/j.carbpol.2012.06.036.
830 (30) Devi, P. G.; Velu, A. S. Synthesis, Structural and Optical Properties of Pure ZnO and Co
831 Doped ZnO Nanoparticles Prepared by the Co-Precipitation Method. J. Theor. Appl. Phys.
832 2016, 10 (3), 233–240. https://doi.org/10.1007/s40094-016-0221-0.
833 (31) Roy, S.; Rhim, J.-W. Carrageenan-Based Antimicrobial Bionanocomposite Films
834 Incorporated with ZnO Nanoparticles Stabilized by Melanin. Food Hydrocoll. 2019, 90,
835 500–507. https://doi.org/https://doi.org/10.1016/j.foodhyd.2018.12.056.
836 (32) Klinge, S. A.; Sawyer, G. A. Effectiveness and Safety of Topical versus Oral Nonsteroidal
837 Anti-Inflammatory Drugs: A Comprehensive Review. Phys. Sportsmed. 2013, 41 (2), 64–
838 74. https://doi.org/10.3810/psm.2013.05.2016.
839 (33) Li, H.; Liu, K.; Sang, Q.; Williams, G. R.; Wu, J.; Wang, H.; Wu, J.; Zhu, L.-M. A
840 Thermosensitive Drug Delivery System Prepared by Blend Electrospinning. Colloids
841 Surfaces B Biointerfaces 2017, 159, 277–283.
842 https://doi.org/https://doi.org/10.1016/j.colsurfb.2017.07.058.
843 (34) Li, H.; Sang, Q.; Wu, J.; Williams, G. R.; Wang, H.; Niu, S.; Wu, J.; Zhu, L.-M.; Dual-
844 Responsive Drug Delivery Systems Prepared by Blend Electrospinning. Int. J. Pharm.
845 2018, 543 (1), 1–7. https://doi.org/https://doi.org/10.1016/j.ijpharm.2018.03.009.
846 (35) Wyns, H.; Meyer, E.; Plessers, E.; Watteyn, A.; Van Bergen, T.; Schauvliege, S.; De Baere,
847 S.; Devreese, M.; de Backer, P.; & Croubels, S. Modulation by gamithromycin and
848 ketoprofen of in vitro and in vivo porcine lipopolysaccharide-induced inflammation, Vet.
849 Immunol. Immunopathol. 2015, 168, 211–222.
850 https://doi.org/10.1016/j.vetimm.2015.09.014.

(36) Davies, L.C.; Jenkins, S.J.; Allen, J.E.; Taylor, P.R. Tissue-resident macrophages, Nat. Immunol. 2013, 14, 986–995. https://doi.org/10.1038/ni.2705

(37) Cao, Y., Chen, J., Ren, G., Zhang, Y., Tan, X., & Yang, L. Punicalagin Prevents Inflammation in LPS-Induced RAW264.7 Macrophages by Inhibiting FoxO3a/Autophagy Signaling Pathway. Nutrients, 2019, 11, 2794. https://doi.org/10.3390/nu11112794

(38) Wang, X.;, Khalil, R.A. Matrix Metalloproteinases, Vascular Remodeling, and Vascular Disease. Adv Pharmacol. 2018, 81, 241-330. https://doi.org/10.1016/bs.apha.2017.08.002.

(39) Gomes, B.P.F. de A.; Herrera, D.R. Etiologic role of root canal infection in apical periodontitis and its relationship with clinical symptomatology, Braz. Oral Res. 2018, 32, 82–110. https://doi.org/10.1590/1807-3107bor-2018.vol32.0069.

(40) Barbosa-Ribeiro, M.; Arruda-Vasconcelos, R.; de-Jesus-Soares, A.; Zaia, A.A.; Ferraz, C.C.R.; de Almeida, J.F.A.; Gomes, B.P.F.A. Effectiveness of calcium hydroxide-based intracanal medication on infectious/inflammatory contents in teeth with post-treatment apical periodontitis, Clin. Oral Investig. 2019, 23, 2759–2766. https://doi.org/10.1007/s00784-018-2719-0.

(41) Cui, N.; Hu, M.; Khalil, R.A. Biochemical and Biological Attributes of Matrix Metalloproteinases, Prog. Mol. Biol. Transl. Sci. 2017, 147, 1–73. https://doi.org/10.1016/bs.pmbts.2017.02.005.

(42) Maia, L.M.; Espaladori, M.C.; Diniz, J.M.B.; Tavares, W.L.F.; de Brito, L.C.N.; Vieira, L.Q.; Sobrinho, A.P.R.; Clinical endodontic procedures modulate periapical cytokine and chemokine gene expressions, Clin. Oral Investig. 2020, 24, 3691–3697. https://doi.org/10.1007/s00784-020-03247.

(43) Eder, K.; Baffy, N.; Falus, A.; Fulop, A.K. The major inflammatory mediator interleukin-6 and obesity, Inflamm. Res. 2009, 58, 727–736. https://doi.org/10.1007/s00011-009-0060-4.

(44) Saiki, P.; Nakajima, Y.; Van Griensven, L.J.L.D.; Miyazaki, K. Real-time monitoring of IL-6 and IL-10 reporter expression for anti-inflammation activity in live RAW 264.7 cells, Biochem. Biophys. Res. Commun. 2018, 505, 885–890. https://doi.org/https://doi.org/10.1016/j.bbrc.2018.09.173.

(45) Azuma, M.M.; Samuel, R.O.; Gomes-Filho, J.E.; Dezan-Junior, E.; Cintra, L.T.A. The role of IL-6 on apical periodontitis: A systematic review, Int. Endod. J. 2014, 47, 615–621. https://doi.org/10.1111/iej.12196.

(46) Braz-Silva, P. H.; Bergamini, M. L.; Mardegan, A. P.; De Rosa, C. S.; Hasseus, B., & Jonasson, P. Inflammatory profile of chronic apical periodontitis: a literature review. Acta odontologica Scandinavica. 2019, 77 (3), 173–180. https://doi.org/10.1080/00016357.2018.1521005.

(47) Zilm, P. S.; Butnejski, V.; Rossi-Fedele, G.; Kidd, S. P.; Edwards, S.; Vasilev, K. D-Amino Acids Reduce Enterococcus Faecalis Biofilms in Vitro and in the Presence of Antimicrobials Used for Root Canal Treatment. PLoS One 2017, 12 (2), 1–14. https://doi.org/10.1371/journal.pone.0170670.

(48) Luna, P.; Martínez-Castañon, G.-A.; Zavala-Alonso, V.; Patiño-Marin, N.; Nino, N.; Moran, J.; & Ramírez-González, J.-H. Bactericide Effect of Silver Nanoparticles as a Final Irrigation Agent in Endodontics on Enterococcus faecalis: An Ex Vivo Study. Journal of Nanomaterials, 2016, 1-7. https://doi.org/10.1155/2016/7597295

(49) Sirelkhatim, A.; Mahmud, S.; Seeni, A.; Kaus, N. H. M.; Ann, L. C.; Bakhori, S. K. M.; Hasan, H.; Mohamad, D. Review on Zinc Oxide Nanoparticles: Antibacterial Activity and Toxicity Mechanism. Nano-Micro Lett. 2015, 7 (3), 219–242. https://doi.org/10.1007/s40820-015-0040-x.

(50) Shrestha, A.; Zhilong, S.; Gee, N. K.; Kishen, A. Nanoparticulates for Antibiofilm Treatment and Effect of Aging on Its Antibacterial Activity. J. Endod. 2010, 36 (6), 1030–1035. https://doi.org/10.1016/j.joen.2010.02.008.

(51) Alves, M. J.; Grenho, L.; Lopes, C.; Borges, J.; Vaz, F.; Vaz, I. P.; Fernandes, M. H. Antibacterial Effect and Biocompatibility of a Novel Nanostructured ZnO-Coated Gutta-Percha Cone for Improved Endodontic Treatment. Mater. Sci. Eng. C. 2018, 92, 840–848. https://doi.org/https://doi.org/10.1016/j.msec.2018.07.045.

(52) Andrade, F. B. de; Arias, M. P. C.; Maliza, A. G. A.; Duarte, M. A. H.; Graeff, M. S. Z.; Amoroso-Silva, P. A.; Midena, R. Z.; Moraes, I. G. de. A New Improved Protocol for in Vitro Intratubular Dentinal Bacterial Contamination for Antimicrobial Endodontic Tests: Standardization and Validation by Confocal Laser Scanning Microscopy. J. Appl. Oral Sci. 2015, 23 (6), 591–598. https://doi.org/10.1590/1678-775720140261.

(53) Villette, G.; Manek, S.; Legner, M.; Fillery, E. D.; Torneck, C. D.; Basrani, B.; R.; & Friedman, S. Characterization of an ex vivo model for the assessment of root canal disinfection. Journal of endodontics. 2008, 34 (12), 1490–1496. https://doi.org/10.1016/j.joen.2008.08.038

(54) Sjögren, U.; Figdor, D.; Persson, S.; & Sundqvist, G. Influence of infection at the time of root filling on the outcome of endodontic treatment of teeth with apical periodontitis.

International endodontic journal, 1997, 30 (5), 297–306. https://doi.org/10.1046/j.1365-2591.1997.00092.x.

(55) Siqueira JF Jr, Guimarães-Pinto T, Rôças IN. Effects of chemomechanical preparation with 2.5% sodium hypochlorite and intracanal medication with calcium hydroxide on cultivable bacteria in infected root canals. J Endod. 2007, 33 (7), 800-5. https://doi.org/10.1016/j.joen.2006.11.023.

(56) Porter, M. L. A.; Münchow, E. A.; Albuquerque, M. T. P.; Spolnik, K. J.; Hara, A. T.; Bottino, M. C. Effects of Novel 3-Dimensional Antibiotic-Containing Electrospun Scaffolds on Dentin Discoloration. J. Endod. 2016, 42 (1), 106–112. https://doi.org/10.1016/j.joen.2015.09.013.

Table of Contents graphic

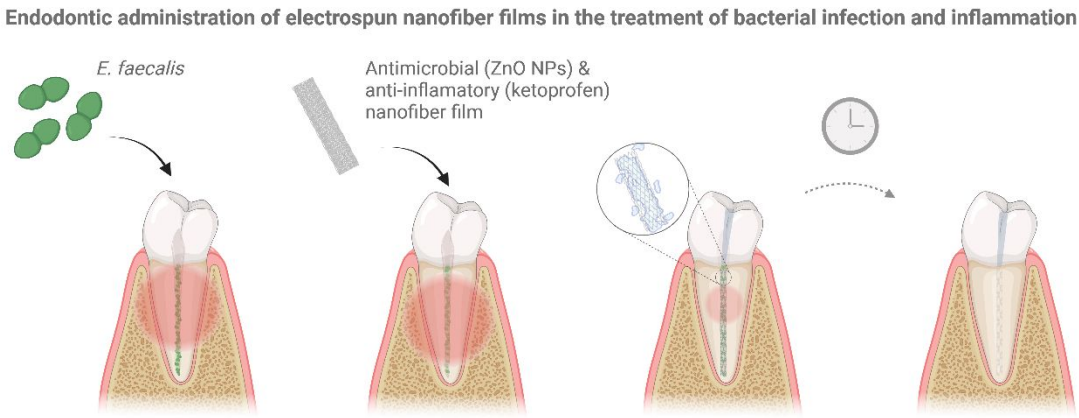

934

935

936